Environ Earth Sci
DOI 10.1007/s12665-015-4173-5

ORIGINAL ARTICLE

# Dust emission modeling for the western border region of Mexico and the USA

**Johana M. Carmona · Ana Y. Vanoye · Fabian Lozano · Alberto Mendoza**

Received: 24 July 2014 / Accepted: 10 February 2015


**Abstract** The border area between northwestern Mexico and the southwestern USA is composed of arid and semi-arid regions that are highly vulnerable to wind erosion. As a result, dust resuspension events take place that result in episodes of high concentrations of fine particulate matter in the atmosphere. In winter, air quality standards on both sides of the border are often exceeded. However, accurate estimates of the emission of windblown dust are rare, particularly for Mexico. In this study, emissions of particulate matter from mineral origin (dust) with an aerodynamic diameter less than 2.5 and 10 μm ($PM_{2.5}$ and $PM_{10}$, respectively) were estimated for the border area for a short winter episode (January 4–12, 2006). For this purpose, a mesoscale meteorological model and a wind erosion model were used. The wind erosion model had a horizontal spatial resolution of 4 km × 4 km and a temporal resolution of 1 h. A georeferenced database of surface conditions obtained from satellite data was used in conjunction with soil parameter digital maps to generate the inputs required by the wind erosion model. The $PM_{10}$ emissions for the entire domain and episode were estimated at $\sim$643 g km$^{-2}$ h$^{-1}$ and the $PM_{2.5}$ emissions were estimated at $\sim$47 g km$^{-2}$ h$^{-1}$. The wind erosion model was subject to three sensitivity tests based on perturbation of the input surface parameters. The model output was more sensitive to changes in soil parameters (soil density and plastic pressure) than to changes in land surface data (leaf area index and fraction of vegetation cover).

**Keywords** Particulate matter · Windblown dust emissions · Dust resuspension · Arid and semi-arid areas

## Introduction

Emissions of particulate matter (PM) have a significant effect on the environment, climate and health. This is particularly the case with emissions of PM with a fraction small enough to remain suspended in the atmosphere for a longer time and that can be inhaled (i.e., particulate matter with an aerodynamic diameter of less than 10 μm, $PM_{10}$). It is estimated that mineral dust is the most common emission source, by mass, of suspended PM in the world's atmosphere (Möller 2010). Mineral PM produced from the wind erosion of exposed soils is an important component of Earth's atmosphere, especially over arid and semi-arid regions where the abundance of PM and strong vertical temperature gradients allow dust to enter the upper layers of the troposphere. From there, dust is transported over long distances (Thomas 2011). Although these particles tend to exist primarily in the coarse mode (PM with an aerodynamic diameter greater than 2.5 μm and less than 10 μm, typically expressed as $PM_{2.5–10}$), particles can also have sizes of less than 0.1 μ. $PM_{10}$ concentrations in arid regions of Africa and Asia reach average values of 200–1000 μg m$^{-3}$, although values over 3000 μg m$^{-3}$ have been recorded (e.g., Draxler et al. 2001; Han et al.

**Electronic supplementary material** The online version of this article (doi:10.1007/s12665-015-4173-5) contains supplementary material, which is available to authorized users.

J. M. Carmona · A. Y. Vanoye · A. Mendoza (✉)
Department of Chemical Engineering, Tecnológico de Monterrey, Campus Monterrey, Ave. Eugenio Garza Sada 2501, 64849 Monterrey, NL, Mexico
e-mail: mendoza.alberto@itesm.mx

F. Lozano
Center for Environmental Quality, Tecnológico de Monterrey, Campus Monterrey, Ave. Eugenio Garza Sada 2501, 64849 Monterrey, NL, Mexico

Published online: 20 February 2015

2012; Wang et al. 2012). Mineral aerosols are highly significant because their most important sources (arid and semi-arid regions) occupy a third of the earth's surface.

Air quality is a continuing problem affecting the main urban centers located near the Mexican–USA border (Muñoz et al. 2012). Although many of the air quality problems that affect these urban centers are related to local anthropogenic emissions, mineral dust resuspension and transport from nearby rural locations can result in high $PM_{10}$ peaks (Choi et al. 2006). Much of the 3400-km-long Mexican–USA border region consists of arid or semi-arid land that is largely rural and/or agricultural (irrigated). The two main regions where mineral dust originates are the Chihuahuan and Sonoran deserts. The Sonoran Desert, in particular, has been classified as the North American desert where the highest temperatures are recorded. Estimated dust emissions from the Sonoran Desert are far less frequent than those from the Sahara and the Asian deserts. Maximum emissions in the Sonoran Desert are in the range of 20–50 g $m^{-2}$ $year^{-1}$, with average values in the range of 10–20 g $m^{-2}$ $year^{-1}$; in the Sahara and in the Asian deserts, maximum values can reach 500–1000 g $m^{-2}$ $year^{-1}$ and average values are in the order of 100–200 g $m^{-2}$ $year^{-1}$ (Chin et al. 2007; Gläser et al. 2012). However, it is still important to properly quantify emissions from dust resuspension in the western border region of Mexico and the USA as inhalation of mineral dust has proven to be an important health issue in the region (e.g., Osornio et al. 1991; Alfaro et al. 1997).

Dust emissions resulting in the production of mineral aerosols from soil grains involve complex, nonlinear processes that are governed by meteorology as well as by the state and property of the land surfaces (Darmenova et al. 2009). Considerable efforts have been devoted to accurate modeling of the production and transport of windblown dust particles at regional and global scales (Ginoux et al. 2001; Wang et al. 2012; Giannadaki et al. 2014). With regard to the western border region of Mexico and the USA, Choi and Fernando (2008) used a modified model based on the work of Liu and Westphal (2001) and Park and In (2003) to estimate the entrainment of soil dust. As assessed by Wang et al. (2012), the scheme used by Choi and Fernando (2008) is not considered to be complex. This study proposes the use of a more advanced scheme to estimate windblown dust emissions for the western border region of Mexico and the USA.

## Methods

### Modeling platform and case study

The calculation of dust emissions was performed through the coupling of a Wind Erosion Model with a Mesoscale Meteorological Model and a surface input parameters database (Fig. 1). The Integrated Wind Erosion Modeling System (IWEMS; Shao 2008), also known as the Computational Environmental Management System (CEMSYS; Shao et al 2010), can produce quantitative predictions of wind erosion from local to global scales. The system has the capacity to model the entire wind erosion process, from the entrainment of particles to their transport and deposition. However, in this study, only the dust module in IWEMS was used to estimate emissions of particulate matter ($PM_{2.5}$ and $PM_{10}$).

IWEMS uses the following formulation to obtain size-resolved dust emissions (Shao 2004):

$$F(d_i, d_s) = c_y \eta_{fi} [(1 - \gamma) + \gamma \sigma_p](1 + \sigma_m) g \frac{Q_{ds}}{u_*^2}, \quad (1)$$

where $F(d_i,d_s)$ is the dust emission rate of particle size $d_i$ (from the $i$-th size bin) generated by the saltation of particles of size $d_s$; $c_y$ is the dust emission coefficient; $\eta_{fi}$ is the

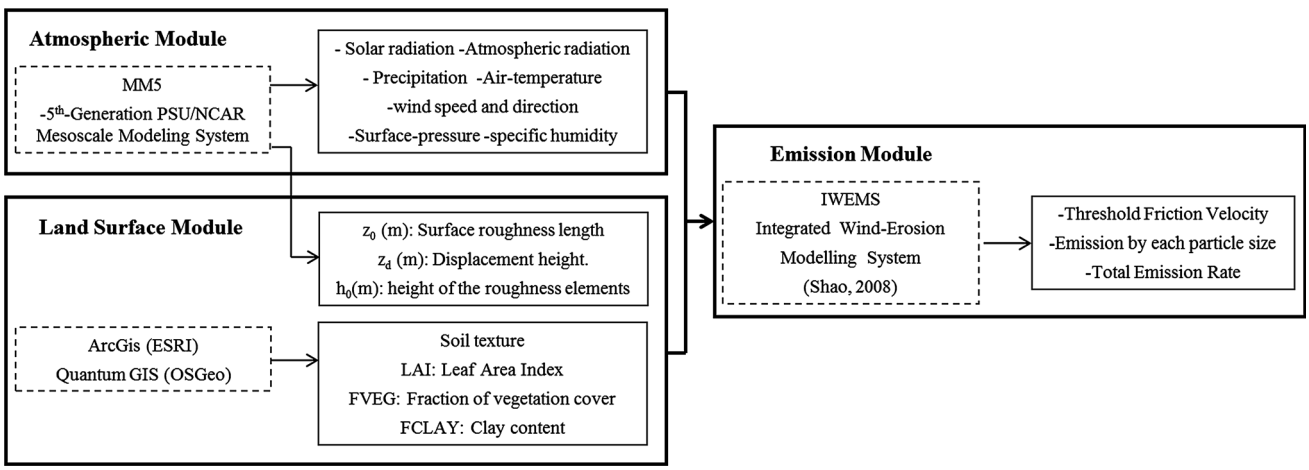


**Fig. 1** *Flow diagram* of computational tools used for modeling windblown dust emissions

fraction of dust that can be emitted; $\gamma$ is a function which describes how easily aggregated dust can be released; $\sigma_p$ is the ratio between the fraction of free dust and that of aggregated dust;$\sigma_m$ is the bombardment efficiency; $g$ is acceleration due to gravity; $Q_{ds} \equiv Q(d_s)$ is the saltation flux of particles of size $d_s$; and the friction velocity $u_*$ is the capacity of wind to generate erosion.

$F(d_i)$, the emission of dust of size $d_i$ associated with the saltation of all grain sizes, is estimated as a weighted average over the sand particle size ($d_1$–$d_2$):

$$F(d_i) = \int_{d_1}^{d_2} F(d_i, d) p_s(d)\, \delta d, \tag{2}$$

and the total dust emission ($F$) is:

$$F = \sum_{i=1}^{I} F(d_i), \tag{3}$$

where $I$ is the total number of bins in which the particle size distribution was divided. This scheme assumes that the particle size distribution of airborne dust [$p_s(d)$] is known. Here, $\delta d$ is used to represent differentiation to avoid confusion with particle size $d$. IWEMS has been successfully used in a number of studies that have addressed the dynamics of dust emission and resuspension in arid environments (Park and Park 2010; Kang et al. 2011; Wang et al. 2013).

Meteorological variables required for the dust emission modeling process (including surface wind velocity) were obtained through the application of the PSU/NCAR Mesoscale Meteorological model (MM5; Grell et al. 1994). Surface data (e.g., soil moisture and vegetation cover) required by IWEMS was developed using both satellite data from the moderate resolution imaging spectroradiometer (MODIS) sensors and soil classification digital maps.

Emissions were estimated for a modeling domain that spanned an area of 394,384 km$^2$ in a 157 × 157 grid cell arrangement (4 km × 4 km grid resolution), covering the states of Arizona and New Mexico in the USA and the states of Sonora and Chihuahua in Mexico (D02 domain in Fig. 2). This region is covered mainly by arid and semi-desert areas (CEC 1997). The aim in this study was to explore the use of the proposed modeling framework to estimate windblown dust emissions to the indicated geographic region, and not to explore seasonal or annual variations of emission estimates. As such, the modeling period was selected to include a short winter episode (January 4–12, 2006). Winter is of particular interest in this region given the low frequency of rain in the season (Choi et al. 2006; ADEQ 1999). In spring, peak concentrations in this area can be influenced by trans-Pacific transport from Asia (Chin et al. 2007). All these factors ensured that the

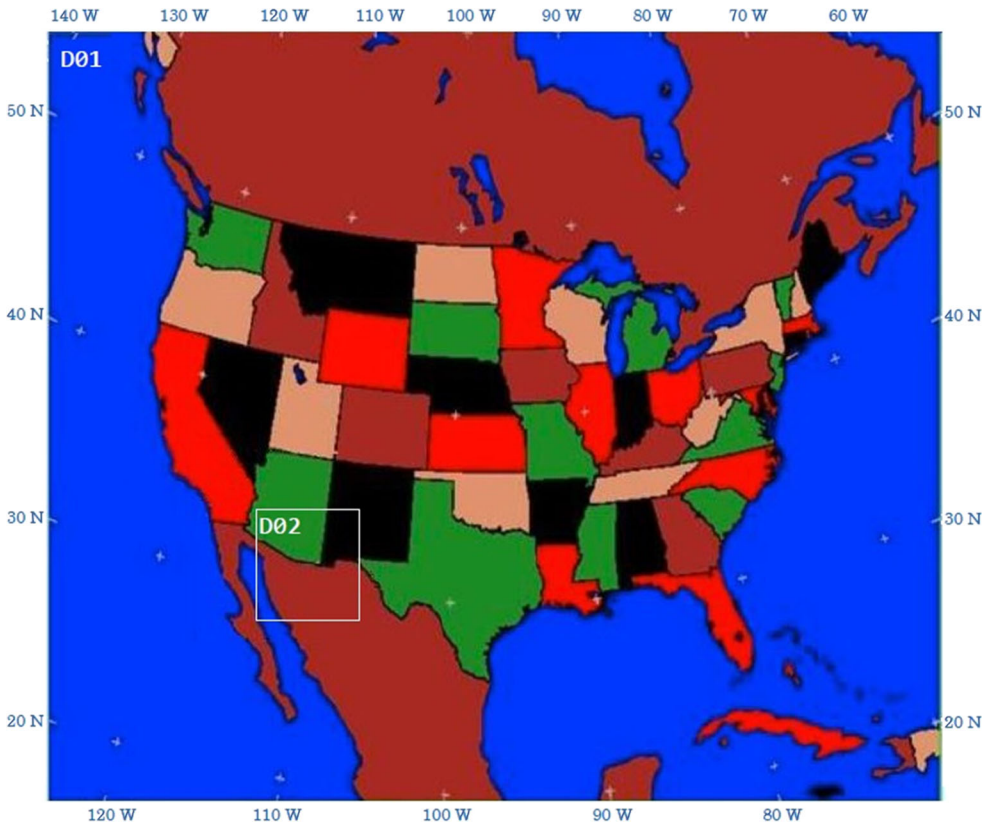


**Fig. 2** MM5 nested modeling domains (meteorological inputs to the wind erosion model were obtained from the D02 subdomain)

results obtained would be suitable for further analyzing the regional impact of local emissions. Emissions for $PM_{2.5}$ and $PM_{10}$ were obtained for average time intervals of an hour.

### Generation of meteorological fields

Input data for MM5 was processed as suggested by Vanoye and Mendoza (2009). In the same way, model setup (boundary conditions, parameterization schemes, sigma pressure levels, data assimilation scheme, etc.) was defined as in similar applications of MM5 to northern Mexico and the southern USA that have given acceptable model performance (Kemball-Cook et al. 2004; Vanoye and Mendoza 2009; Sierra et al. 2013). MM5 generated three-dimensional (3D) meteorological fields for two nested domains (Fig. 2). The innermost domain is identical to the domain defined for the emission estimation procedure. Information from the coarse domain was passed to the inner domain using one-way nesting. The meteorology–chemistry interface processor (MCIP; Otte and Pleim 2010) was used to extract and process the specific inputs required by IWEMS: wind speed, wind direction, short wave solar radiation, long wave atmospheric radiation, precipitation, air temperature, surface pressure, and specific humidity for each grid cell.

### Land surface data

Surface input parameters required by IWEMS were obtained using two data sets. The first data set consisted of unique values (constants) which were applied to the entire computational grid. Soil density and plastic pressure were given the values of 1,000 kg $m^{-3}$ and 20,250 N $m^{-2}$, respectively, as suggested by Shao et al. (2011). These base case values were then subjected to a sensitivity analysis test in which values of 1,700 kg $m^{-3}$ and 50,000 N $m^{-2}$ were defined for soil density and plastic pressure, respectively. These last values were the highest values reported in NRCS (2005) for the soil types found in the US domain. The sensitivity analysis was performed following a "brute-force" approach: the wind erosion model was run changing one parameter of interest at a time.

The second data set was constructed with land surface values that changed spatially and for which a geographic information system was generated. Variables included in this data set comprised the following: roughness length ($Z_o$), zero-displacement height or vertical displacement ($Z_d$), vegetation height ($h_o$), leaf area index (LAI), fraction of vegetation cover (FVEG), and fraction of clay in the soil (FCLAY).

$Z_d$ was estimated as 0.7 times $Z_o$ (Gryning and Schiemeier 2001), $Z_o$ was obtained directly from MM5 output, and $h_o$ was estimated from (Espert and López 2004):

$$h_o = \left(\frac{Z_o}{0.056}\right)^{0.73}. \quad (4)$$

LAI is one of the most useful parameters for characterizing vegetation cover. It is defined as units of green leaf surface per unit surface area (Hufkens et al. 2008; Tillack et al. 2014). LAI is also used to evaluate soil moisture indirectly using remote sensing tools (Yilmaz et al. 2008). FVEG can also be estimated using remote sensing tools. In this work, FVEG was estimated by determining the fraction of photosynthetically active radiation (FPAR), as it has been argued that there is a 1:1 relationship between FVEG and FPAR (Burstall and Harris 1983; Millard et al. 1990). Particularly, MOD 15 LAI and FPAR data from January 12, 2006 was used to obtain LAI and FVEG values, as these products have been used extensively as satellite-derived parameters for calculation of land surface data.

The MOD 15 LAI and FPAR satellite products are created by compositing maximum values of both LAI and FPAR for 8 day periods. These products have been processed with the MODIS LAI/FPAR algorithm that exploits the spectral content provided by the MODIS instrument onboard the Terra satellite of the United States National Aeronautics and Space Administration. (NASA 2012). Biophysical values are stored in their digital form ($D$) with a scale factor (gain, $G$) and an offset ($O$) that are needed to transform the stored values to their analysis form ($A$). The expression used to decode the digital values contained in each pixel to their analysis form follows the hierarchical data format conventions and can be represented as:

$$A = G \times (D - O). \quad (5)$$

Given that the MOD15 products have a spatial resolution of 1 km and normalized pixel sizes of 250 m × 250 m, it was necessary to select a representative value of LAI and FPAR to assign to each of the 4 km × 4 km cells defined in the modeling domain. This representative value was based on the values of the pixels contained in each cell. In the base case scenario, the statistical majority value contained in each computational cell was selected for estimating LAI and FPAR. In addition, the average value was selected to test the sensitivity of the estimated emissions to this choice.

A prior set of particle size bins (0.2, 0.4, 0.6, 0.85, 1.5, 2.5, 4.0, 6.0, 8.5, and 10 μm) was used to represent the dust particles size. The dust emission modeling was performed based on the clay content assuming that the soil particles with a diameter of less than 10 μm are mostly contained in this kind of soil texture (Shao 2008). The clay percentage was estimated based on the clay content from each type of soil as suggested by the National Institute of Statistics and Geography (INEGI 1998). The FCLAY was estimated in each grid cell using digital maps

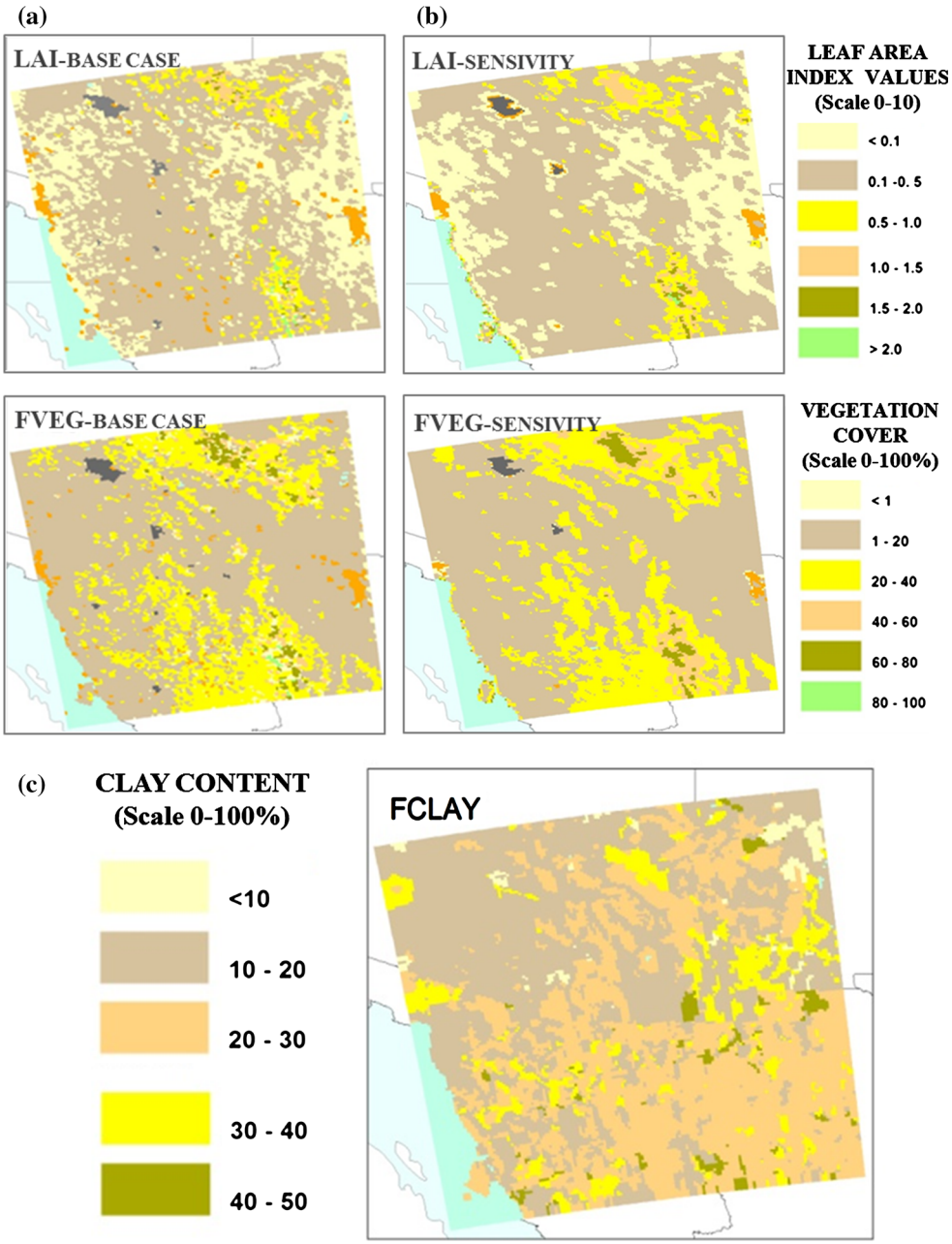


**Fig. 3** Prevailing surface conditions for the model: **a** LAI and FVEG values for the base case, calculated using statistical majority data; **b** LAI and FVEG values for the base case, calculated using average data; **c** FCLAY, fraction of clay in the entire domain, estimated based on the clay content from each type of soil

from Mexico and the USA. For the Mexican side of the computational domain, FCLAY was estimated based on pedological maps (scales 1:250.000 and 1:1.000.000) from the National Institute of Forestry, Agricultural, and Livestock Research (INIFAP) and the National Commission for the Knowledge and Use of Biodiversity (INEGI 1998; CONABIO 2001). For the US side, the FCLAY data were obtained from "The U.S. General Soil Map" (scale 1:250.000) and small-scale soil geography digital soil databases for general soil maps (STATSGO) from the Department of Agriculture, Natural Resources Conservation Service (NRCS 2005).

## Results

### Land surface conditions

Prevailing surface conditions for the modeled episode were characterized by LAI values <1, i.e., low soil moisture and vegetation cover <20 % (Fig. 3a). These conditions favor the resuspension of fine particulate matter (Draxler et al. 2010; He et al. 2011). Clay content in the domain was less than 50 %; most cells had values in the 30–40 % range (Fig. 3c). Particle size distribution determines the main emission mechanism (Gillette et al. 1982). Particulates

emitted in soils with clay texture tend to be suspended (Shao 2008). Thus, the conditions reduced the threshold friction velocity calculated by the erosion model and therefore favored dust resuspension.

## Emissions inventory

The total emissions inventory was 2,221 kg for $PM_{10}$ and 162 kg for $PM_{2.5}$. Domain-wide emissions of resuspended PM for the entire modeled episode are presented in Table 1. Figure 4 summarizes the daily domain-wide emissions inventory of $PM_{10}$ and $PM_{2.5}$. A similar daily trend was observed for both $PM_{10}$ and $PM_{2.5}$. For the entire domain and episode, average $PM_{10}$ emissions were estimated as being $\sim$643 g km$^{-2}$ h$^{-1}$; $PM_{2.5}$ emissions were on average $\sim$47 g km$^{-2}$ h$^{-1}$. These results fall within the range obtained by Chin et al. (2007), who estimated an average emission between 570 and 1140 g km$^{-2}$ h$^{-1}$ for the same region. Although the average of the daily $PM_{10}$/$PM_{2.5}$ emissions ratio was 13.5 $\pm$ 0.8 (on average, $PM_{2.5}$ emissions accounted for 7 % of the $PM_{10}$ emissions), the daily $PM_{10}$/$PM_{2.5}$ emissions ratio ranged between 3.4 and 14.8 (roughly between 6.8 and 29.4 %). These ratios compared well with ratios used by emission factor techniques. Emission factor techniques used to derive emission estimates typically assign a constant value to the $PM_{10}$/$PM_{2.5}$ ratio for a given source, including windblown dust. Such is the case, for example, with the AP-42 compendium of the United States Environmental Protection Agency (Davis 2000; Mueller et al. 2013). However, these methodologies suffer from the fact that the $PM_{10}$/$PM_{2.5}$ emission ratio has to be calibrated empirically as the region of application changes (e.g., WRAP 2006). For example, in Davis (2000) a value of 3.3 is suggested for the $PM_{10}$/$PM_{2.5}$ ratio, whereas in WRAP (2006) a value of 6.6 is suggested. The methodology used in this study is superior as the emission estimation procedure is not restricted by a constant $PM_{10}$/$PM_{2.5}$ ratio.

**Table 1** Emissions inventory for the entire episode (kg)

| | $PM_{10}$ | $PM_{2.5}$ |
|---|---|---|
| Total episodes of emissions | 2,221 | 162 |
| Daily average | 247 | 18 |
| Standard deviation | 226 | 17 |

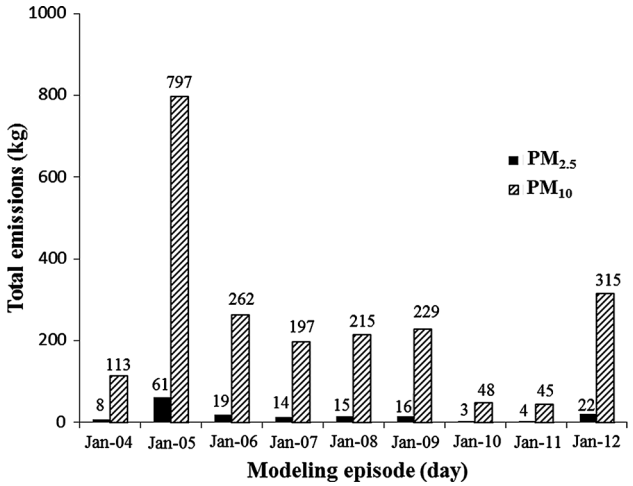


**Fig. 4** Domain-wide daily emissions of $PM_{2.5}$ and $PM_{10}$

The amount of mass emitted for each particle size depended mainly on wind speed. As with a study carried out by Marticorena et al. (1997), it was observed that large particles were mostly emitted at low wind speeds; small particles were emitted as wind speed increased. In this study, the threshold friction velocity was found to be 0.5 m s$^{-1}$. The particles were emitted at maximum wind velocities between 8.7 and 17.8 m s$^{-1}$.The wind velocity distribution had a log-normal behavior and was similar for each episode day, with a daily geometric mean ($\mu_g$) between 2.74 and 4.62 and a daily geometric standard deviation ($\sigma_g$) between 1.74 and 1.80 (Fig. 5).

One limitation of this study is the lack of observational surface emissions data or enough rural air monitoring stations in the region to make any extensive comparisons with the modeling results obtained here. In fact, there is a complete lack of air quality monitoring stations at rural locations in the Mexican side of the domain. However, a preliminary analysis was conducted to compare the simulated hourly dust emissions (g km$^{-2}$) with surface hourly $PM_{10}$ concentrations (μg m$^{-3}$) data reported at one monitoring station. The analysis can be found in the Supplementary Material (SM) accompanying this article. As a result of this comparison, a moderate correlation ($r^2 = 0.48$) was obtained for the entire modeling period. It is clear that other issues including variation in aerosol type, other source contributions, and transport dynamics must be completely understood before establishing a relationship between emissions and concentrations. In addition to the correlation analysis, the time series of $PM_{10}$ concentrations along with time series of simulated $PM_{10}$ emissions were analyzed. The results indicate a similar temporal behavior between predicted emissions and observed concentrations. Results indicate that, considering the 4-km domain, the model was able to replicate with reasonable accuracy some events of high $PM_{10}$ concentrations.

## Sensitivity analysis

Three sensitivity tests were conducted to probe the response of the emissions model to independent changes in soil parameters (density and plastic pressure) and land surface data (LAI and FVEG). January 8, 2006 was chosen

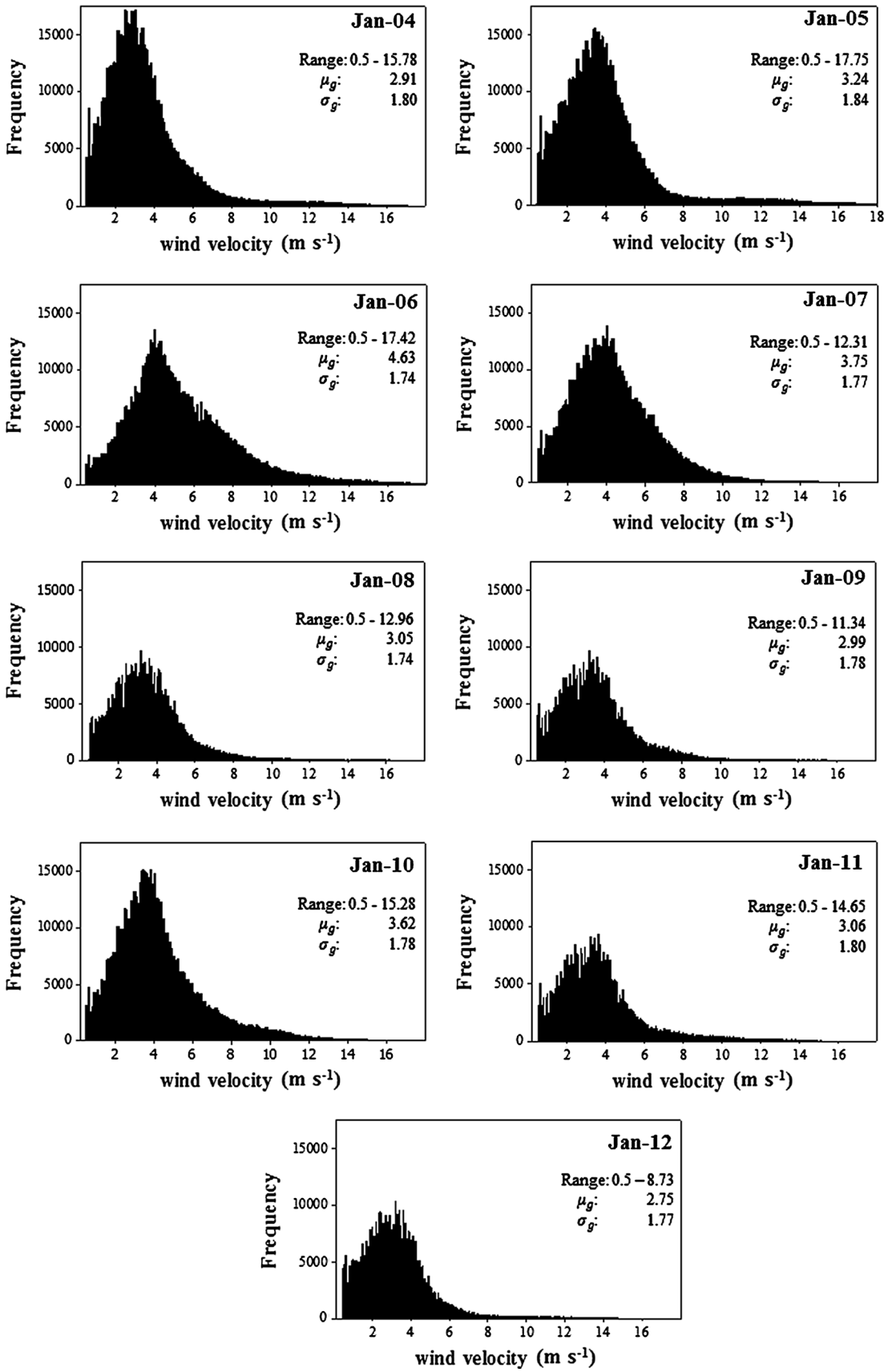


**Fig. 5** Domain-wide daily wind velocity distribution plots based on average time intervals of an hour

**Table 2** Emissions inventory for each sensitivity test and its variation with respect to the base case

| | $PM_{10}$ | | $PM_{2.5}$ | |
|---|---|---|---|---|
| | Emissions (kg $day^{-1}$) | Difference[a] (%) | Emission (kg $day^{-1}$) | Difference[a] (%) |
| Base case | 214.85 | – | 15.02 | – |
| Density change scenario | 242.42 | +12.83 | 17.00 | +13.16 |
| Pressure change scenario | 195.80 | −9.87 | 13.66 | −9.08 |
| LAI–FVEG change scenario | 220.41 | +2.59 | 15.33 | +1.93 |

[a] Compared to the base case (i.e., sensitivity scenario minus base case)

as the day to perform the sensitivity analysis tests. On this day, the daily domain-wide emissions were close to the episode average and the distribution of wind velocities was less dispersed than on other days. The wind velocity geometric standard deviation was 1.74, which was the smallest in the episode (Fig. 5).

Prevailing surface conditions for the LAI sensitivity test were similar to base case conditions: LAI values <1. However, an increase in data points in the 0.1–0.5 interval was observed, together with a decrease in data points in the 0.5–1.0 interval (Fig. 3b). The main effect was an overall decrease in soil moisture content. For the FVEG sensitivity test, an increase in the spatial distribution of vegetation cover in the 20–40 % range and the 40–60 % range was observed. As FVEG increases, emissions tend to be lower.

Table 2 presents the domain-wide emissions estimated for January 8 for the base case and the sensitivity tests. In general, the model was more sensitive to the prescribed changes in the soil parameters (density and plastic pressure) than to the changes implemented in the land surface data (LAI and FVEG). An increase of 70 % in the soil density (relative to the base case) increased domain-wide emissions by approximately 13 % on the selected day. With regards to the plastic pressure of the soil, an increase of 150 % (relative to the base case) resulted in emissions being reduced by approximately 10 %. Changes were very similar between the $PM_{10}$ and $PM_{2.5}$ fractions. These results indicate that refining these input variables would result in changes to the model output of approximately ±15 %. In some cases, error cancelation can occur. With regard to the LAI and FVEG sensitivity scenario, an increment on the emissions inventory of approximately 3 % with respect to the base case was obtained using LAI and FVEG average values.

Figure 6a shows that the main changes in emissions occurred in the northern part of the domain. On this day, 88 % of the emission sources were located on the US side, where LAI <1, FVEG <40, and wind velocities between 5 and 12 m $s^{-1}$ were the predominant conditions. Spatial analysis of the sensitivity tests was conducted by generating comparative maps (Fig. 6b) in which the emissions from each computational cell from the base case were subtracted from the emissions from the corresponding cell in the different sensitivity scenarios (i.e., for each cell: $PM_{\text{sensitivity scenario}}$–$PM_{\text{base case}}$). Thus, a positive value indicates an increase in PM emissions with respect to the base case and a negative value a reduction with respect to the base case. For the particular case of the LAI–FVEG sensitivity scenario, particulate matter emissions increased (as expected) when LAI and FVEG attained low values, i.e., LAI <1 and FVEG <20 % (low moisture content and poor vegetation cover). In this scenario, LAI and FVEG values for each cell of the entire modeling grid changed. As a result, greater spatial variability was observed in the emission sources (compared to the soil parameter sensitivity tests) as the threshold friction velocity is a function of both soil moisture and vegetation cover (Draxler et al. 2010). Additional information on sources input and model performance analysis for the emission model in the base case and in the sensitivity scenarios can be found in the SM.

## Conclusions

The emissions inventory for the entire domain was ~643 g $km^{-2}$ $h^{-1}$ of $PM_{10}$ and ~47 g $km^{-2}$ $h^{-1}$ of $PM_{2.5}$. Prevailing soil conditions in the domain, represented by low moisture content, vegetation cover of less than 20 %, and clay content (30–40 %), favored the process of particle emission through wind resuspension. The geographical distribution of the emission sources varied throughout the episode as emissions occurred in places where the weather and surface conditions combined to reach the threshold friction velocity. Compared to the base case, the emissions inventory had a variation of ±13 % in the pressure and density sensitivity tests. However, there was no change in the main location of the emission sources in these scenarios, as the soil parameters were subject to the same domain-wide perturbation. Finally, the LAI and FVEG sensitivity test resulted in a variation of the emissions inventory of less than 3 %. In this scenario, a greater spatial variability in the source strength was observed as

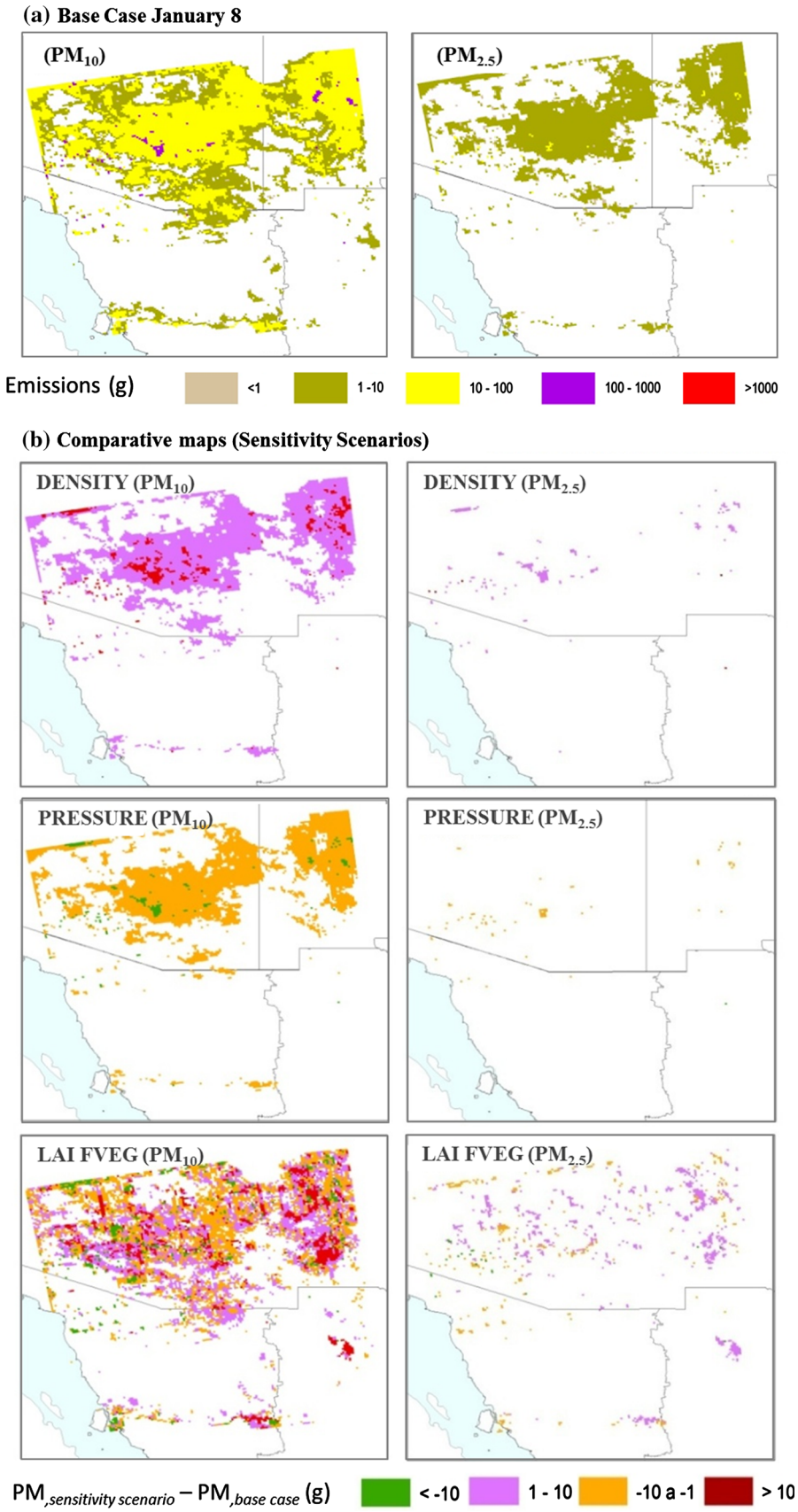


**Fig. 6** Comparison of emission sources behavior and emission difference for $PM_{10}$ and $PM_{2.5}$ between the base case and the sensitivity scenario (January 8)

each modeling grid cell was subject to the prescribed changes in the sensitivity test.

**Acknowledgments** This work was supported by Tecnológico de Monterrey through Grant 0020CAT186. J. Carmona further acknowledges the support (scholarship) received from Mexico's National Council for Science and Technology (CONACYT) during her research stay at Tecnológico de Monterrey. The authors gratefully acknowledge Dr. Yaping Shao from the University of Hong Kong for providing the dust emission module used in this work.

## References

ADEQ, Arizona Department of Environmental Quality (1999) Douglas/Agua Prieta air pollution study protocol. Memorandum AQD:AAS: EVAL:PGH:222-8-17-99. Phoenix, Arizona

Alfaro E, Flores G, Harta F, de la Orozco HA, Quintana R, Osornio AR (1997) In vitro induction of abnormal anaphases by contaminating atmospheric dust from the city of Mexicali, Baja California, Mexico. Arch Med Res 28(4):549–553

Burstall L, Harris PM (1983) The estimation of percentage light interception from leaf area index and percentage ground cover in potatoes. J Agri Sci 100(01):241–244

CEC, Commission for Environmental Cooperation (1997) Ecological regions of North America toward a common perspective. Communications and Public Outreach Department of CEC Secretariat. Montreal, Quebec, Canada

Chin M, Diehl T, Ginoux P, Malm W (2007) Intercontinental transport of pollution and dust aerosols: implications for regional air quality. Atmos Chem Phys 7:5501–5517. doi:10.5194/acp-7-5501-2007

Choi YJ, Fernando H (2008) Implementation of a windblown dust parameterization into MODELS-3/CMAQ: application to episodic PM events in the US/Mexico border. Atmos Environ 42(24):6039–6046. doi:10.1016/j.atmosenv.2008.03.038

Choi YJ, Hydeb P, Fernando H (2006) Modeling of episodic particulate matter events using a 3-D air quality model with fine grid: applications to a pair of cities in the US/Mexico border. Atmos Environ 40(27):5181–5201. doi:10.1016/j.atmosenv.2006.04.025

CONABIO, National Commission for the Knowledge and Use of Biodiversity (2001) Pedological map. http://www.conabio.gob.mx-/informacion/gis/. Accessed 26 Apr 2012

Darmenova K, Sokolik IN, Shao Y, Marticorena B, Bergametti G (2009) Development of a physically based dust emission module within the weather research y forecasting (WRF) model: assessment of dust emission parameterizations and input parameters for source regions in Central and East Asia. J Geophys Res. doi:10.1029/2008JD011236

Davis WT (2000) Air pollution engineering manual. Wiley, New York, pp 117–135

Draxler R, Gillette D, Kirkpatrick J, Heller J (2001) Estimating $PM_{10}$ air concentrations from dust storms in Iraq, Kuwait and Saudi Arabia. Atmos Environ 35(25):4315–4330. doi:10.1016/S1352-2310(01)00159-5

Draxler R, Ginoux P, Stein A (2010) An empirically derived emission algorithm for wind-blown dust. J Geophys Res. doi:10.1029/2009JD013167

Espert V, López A (2004) Dispersión de contaminantes en la atmósfera. 1st edn. Universidad Politécnica de Valencia, España. Spanish version Alfaomega editors, Mexico

Giannadaki D, Pozzer A, Lelieveld J (2014) Modeled global effects of airborne desert dust on air quality and premature mortality. Atmos Chem Phys 14:957–968. doi:10.5194/acp-14-957-2014

Gillette D, Adams J, Muhs D, Kihl R (1982) Threshold friction velocities and rupture moduli for crusted desert soils for the input of soil particles into the air. J Geophys Res 87(C11):9003–9015

Ginoux P, Chin M, Tegen I, Prospero J, Holben B, Dubovik O, Lin S (2001) Sources and distributions of dust aerosols simulated with the GOCART model. J Geophys Res 106(D17):20255–20273

Gläser G, Kerkweg A, Wernli H (2012) The mineral dust cycle in EMAC 2.40: sensitivity to the spectral resolution and the dust emission scheme. Atmos Chemis Phys 12:1611–1627. doi:10.5194/acp-12-1611-2012

Grell GA, Dudhia J, Stauffer DR (1994) A description of the Fifth-Generation Penn State/NCAR Mesoscale Model (MM5). NCAR Technical Note, NCAR/TN-398+STR. Boulder, CO. doi:10.5065/D60Z716B

Gryning S, Schiemeier F (2001) Air pollution modeling and its application XIV. Kluwer Academic/Plenum Publishers, New York

Han X, Ge C, Tao J, Zhang M, Zhang R (2012) Air quality modeling for a strong dust event in East Asia in March 2010. Aerosol Air Qual Res 12:615–628. doi:10.4209/aaqr.2011.11-.0191

He Q, Yang X, Mamtimin A, Tang S (2011) Impact factors of soil wind erosion in the center of Taklimakan Desert. J Arid Land 3(1):9–14. doi:10.3724/SP.J.1227.2011.00009

Hufkens K, Bogaert J, Dong QH, Lu L, Huang CL, Ma MG, Ched T, Li X, Veroustraete F, Ceulemans R (2008) Impacts and uncertainties of upscaling of remote-sensing data validation for a semi-arid woodland. J Arid Environ 72:1490–1505. doi:10.1016/j.jaridenv.2008.02.012

INEGI, Mexico's National Institute of Statistics and Geography (1998) Perfiles de suelos un recorrido por los suelos de Mexico. Banco de Informacion sobre Perfiles de Suelo. Aguas calientes, México

Kang JY, Yoon SC, Shao Y, Kim SW (2011) Comparison of vertical dust flux by implementing three dust emission schemes in WRF/Chem. J Geophys Res Atmos. doi:10.1029/-2010JD014649

Kemball-Cook S, Jia Y, Emery C, Morris R, Wang Z, Tonnesen G (2004) 2002 annual MM5 simulation to support WRAP CMAQ visibility modeling for the Section 308 SIP/TIP: MM5 sensitivity simulations to identify a more optimal MM5 configuration for simulating meteorology in the Western US. Western Regional Air Partnership, California

Liu M, Westphal DL (2001) A study of the sensitivity of simulated mineral dust production to model resolution. J Geophys Res Atmos 106(16):18099–18112. doi:10.1029/2000JD900711

Marticorena B, Bergametti G, Aumont B, Callot Y, N'Doume C, Legrand M (1997) Modeling the saharan dust cycle: 2. Simulation of saharan dust sources. J Geophys Res Atmos 102(D4):4387–4404. doi:10.1029/96JD02964

Millard P, Wright GG, Adams MJ, Birnie RV, Withworth P (1990) Estimation of light interception and biomass of the potato (Solanumtuberosum L.) from reflection in the red and near-infrared spectral bands. Agric For Meteorol 53(1–2):19–31. doi:10.1016/01681923(90)90121-L

Möller D (2010) Chemistry of the climate system. Walter de Gruyter GmbH & Co. KG, New york

Mueller SF, Mallard JW, Mao Q, Shaw SL (2013) Fugitive particulate emission factors for dry fly ash disposal. J Air Waste Manag Assoc 63(7):806–818

Muñoz G, Quintero M, Pumfrey Ross (2012) Air quality at the US-Mexican border: current state and future considerations toward sustainable The US Mexican border environment: binational air

quality management. SCERP MONOGRAPH SERIES 16: 219–265. California, US

NASA, National Aeronautics and Space Administration (2012) Level-4 MODIS global leaf area index (LAI) and fraction of photosynthetically active radiation (FPAR) product. USGS Earth Resources Observation and Science Center. http://glovis.usgs.gov/ Accessed 22 Feb 2014

NRCS, Natural Resources Conservation Service (2005) Soil survey staff United States department of agriculture. Soil survey geographic (SSURGO). Database for Arizona New Mexico. http://datagateway.nrcs.usda.gov/ Accessed 29 Jul 2011

Osornio AR, Hernandez NA, Yanez AG, Ussler W, Overby LH, Brody AR (1991) Lung cell toxicity experimentally induced by a mixed dust from Mexicali Baja California Mexico. Environ Res 56(1):31–47. doi:10.1016/S0013-9351(05)80107-0

Otte TL, Pleim JE (2010) The meteorology-chemistry interface processor (MCIP) for the CMAQ modeling system: updates through MCIPv3.4.1. Geosci Model Dev 3:243–256. doi:10.5194/gmd-3-243-2010

Park S, In H (2003) Parameterization of dust emission for the simulation of the yellow sand (Asian dust) event observed in March 2002 in Korea. J Geophys Res Atmos 108(D19):4618. doi:10.1029/2003JD003484

Park YK, Park SH (2010) Development of a new wind-blown-dust emission module using comparative assessment of existing dust models. Part Sci Technol 28(3):267–286. doi:10.1080/02726351.2010.491761

Shao Y (2004) Simplification of a dust emission scheme and comparison with data. J Geophys Res Atmos 109(D10):202. doi:10.1029/2003JD004372

Shao Y (2008) Physics and modeling of wind erosion, 2nd edn. Springer, Berlin

Shao Y, Ishizuka M, Mikami M, Leys J (2011) Parameterization of size-resolved dust emission and validation with measurements. J Geophys Res Atmos 116(D08):203. doi:10.1029/2010JD014527

Shao Y, Fink AH, Klose M (2010) Numerical simulation of a continental-scale Saharan dust event. J Geophys Res Atmos 115(D13):205. doi:10.1029/2009JD012678

Sierra A, Vanoye A, Mendoza A (2013) Ozone sensitivity to its precursor emissions in northeastern Mexico for a summer air pollution episode. J Air Waste Manag Assoc 63(10):1221–1233. doi:10.1080/10962247.2013.813875

Thomas D (2011) Arid zone geomorphology: Process form and change in drylands, 3rd edn. Oxford, UK

Tillack A, Clasen A, Kleinschmit B, Förster M (2014) Estimation of the seasonal leaf area index in an alluvial forest using high-resolution satellite-based vegetation indices. Remote Sens Environ 141:52–63. doi:10.1016/j.rse.2013.10.018

Vanoye A, Mendoza A (2009) Mesoscale meteorological simulations of summer ozone episodes in Mexicali and Monterrey Mexico: analysis of model sensitivity to grid resolution and parameterization schemes. Water Air Soil Pollut 9:185–202. doi:10.1007/s11267-009-9205-2

Wang K, Zhang Y, Nenes A, Fountoukis C (2012) Implementation of dust emission and chemistry into the community multiscale air quality modeling system and initial application to an Asian dust storm episode. Atmos Chem Phys 12:10209–10237. doi:10.5194/acp-12-10209-2012

Wang JY, Wang SG, Yang Y, Li Y, Guo YT (2013) Application of four schemes for sand and dust emissions in China. Appl Mech Mater 295:1654–1658

WRAP, Western Regional Air Partnership (2006) WRAP fugitive dust handbook. Western Governors' Association, WGA contract 30204-111, Westlake Village, pp 1–26

Yilmaz MT, Hunt ER, Goins LD, Ustin SL, Vanderbilt VC, Jackson TJ (2008) Vegetation water content during SMEX04 from ground data and Landsat 5 thematic mapper imagery. Remote Sens Environ 112:350–362. doi:10.1016/j.rse.2007.03.029